JTTEES 1: 155-160

Microstructural Evaluation of Tungsten Carbide-Cobalt Coatings

J. Nerz, B. Kushner, and A. Rotolico

Tungsten carbide-12 wt.% cobalt coatings were deposited using optimized high-energy plasma (HEP) and high-velocity oxygen fuel (HVOF) thermal spray techniques. The coatings were evaluated using transmission electron microscopy, differential thermal analysis, X-ray diffraction, and subjected to wear tests to relate the coating structure to wear performance. Coatings were evaluated in the as-sprayed condition, as well as after heat treatments in inert atmosphere. The results indicate that a substantial amount of amorphous matrix material is created during the thermal spray process. Carbon and tungsten, liberated through the dissociation of the WC, combine with cobalt present in the starting powder to form amorphous material on solidification. Differential thermal analysis revealed an exothermic reaction for both the HVOF and HEP coatings at approximately 853 and 860 °C, respectively, which did not occur for the powder. Post-coating heat treatment in an inert atmosphere resulted in the recrystallization of the amorphous material into Co_6W_6C and Co_2W_4C, which was dependent on the time and temperature of the heat treatment. Wear testing showed improvement in the wear performance for coatings that were subjected to the heat treatment. This was related to the recrystallization of the amorphous matrix into eta phase carbides.

1. Introduction

THERMAL sprayed tungsten carbide hardface coatings are used for a wide range of applications spanning both the aerospace and other industrial markets. Major aircraft engine manufacturers and repair facilities use hardface coatings for original engine manufacture (OEM), as well as the overhaul of critical engine components. The principal function of these coatings is to resist severe wear environments for such wear mechanisms as abrasion, adhesion, fretting, and particle erosion. Other uses of thermal spray coating technology in the gas turbine industry include the deposition of ceramic thermal barrier coatings to resist heat transfer and friable abradable coatings to provide gas path seals.

The properties and performance of tungsten carbide coatings is attributed to a complex function of carbide size, shape, and distribution, matrix hardness and toughness, and solution of carbon in the cobalt matrix. Previous investigations have concentrated on determining the cause and effect relationships of various deposition processes and coating attributes related to the general coating structure and wear performance. A coating must retain a large volume fraction of finely distributed tungsten monocarbide (WC) to achieve the optimum wear properties. This is largely dependent on the minimizing of decarburization of WC, which can readily occur at the high temperatures associated with the thermal spray process according to the following reactions:

$$2WC \rightarrow W_2C + C \quad [1]$$

$$W_2C \rightarrow 2W + C \quad [2]$$

This reaction is kinetically driven, *i.e.*, time and temperature dependent, with the degree of decarburization being related to the manufacturing method of the starting powder and by the deposition process flame temperature and flame velocity.[1-3] The decomposition reaction may be minimized by limiting the flame temperature and increasing the flame velocity. High-energy plasma (HEP) and high-velocity oxygen fuel (HVOF) processes have been developed to achieve the optimum flame conditions for deposition of WC-Co coatings.

Although decarburization can be reduced by adjusting the flame condition, it cannot be totally eliminated. The liberation of carbon through the decarburization reactions results in two possibilities—oxidation of the carbon according to

$$2C + O_2 \rightarrow 2CO\,(gas) \quad [3]$$

or the diffusion of carbon into the matrix material. Little work has been done to determine what the effect of carbon diffusion has on the matrix properties. The condition and amount of matrix material can have a strong influence on the wear properties of the coating. This investigation focused on the determination of the microstructural composition of the "matrix" material of thermally sprayed WC-Co coatings relative to the effect of carbon diffusion.

Key Words: amorphous matrix, differential thermal analysis (DTA), thermal spray coatings, transmission electron microscopy (TEM), tungsten carbide-cobalt, x-ray diffraction (XRD)

J. Nerz, **B. Kushner**, and **A. Rotolico**, Metco/Perkin Elmer, Westbury, New York.

Editor's Note: This paper was presented at the 4th National Thermal Spray Conference, Pittsburgh, 6-10 May, 1991. The proceedings of this conference will be published by ASM International. Dr. **T.F. Bernecki** is the Editor of these proceedings.

2. Experimental

The powder used for this study was a fused and crushed tungsten carbide-12 wt.% cobalt material commonly used in the aircraft gas turbine industry. Table 1 summarizes the main characteristics of this powder including the nominal chemical composition, particle shape, and average particle size. The par-

Table 1 Starting Powder Characteristics

Nominal composition	Manufacturing process	Particle shape	Average particle size, μm
88 wt.% ($WC + W_2C$) – 12 wt.% Co	Fused/crushed	Angular	13

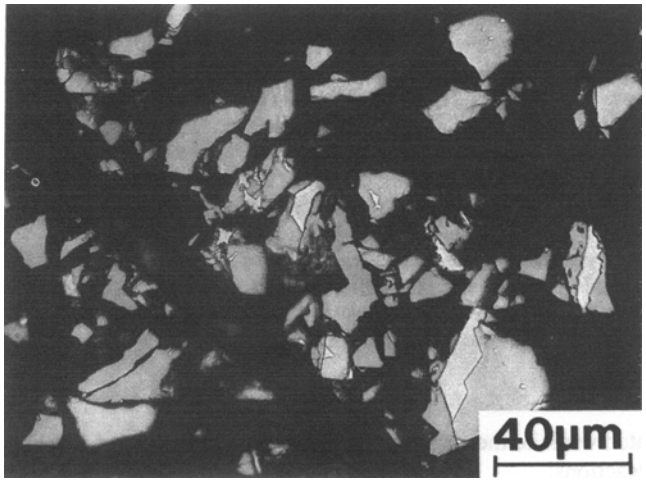

Figure 1 Optical photomicrograph of a cross section of the fused and crushed tungsten carbide-cobalt starting powder. The dark gray phases represent the tungsten carbide crystals, whereas the light regions represent the cobalt binder.

ticle size was determined by a laser light-scattering technique and the size is given in microns. Figure 1 illustrates the particle morphology, demonstrating the angular particle shape as well as the distribution of the dark gray carbide phase and light gray cobalt phase.

The HVOF deposition process involves the combustion of oxygen and a fuel gas in a nozzle designed to produce extremely high-flame velocities. This study utilized the Metco Diamond Jet (DJ) system. The gun has a fairly simple design with an interchangeable nozzle located at the front end, through which a controlled flow of oxygen/fuel gas and compressed air is passed. The gases flow through a siphon system where the fuel and oxygen are thoroughly mixed. The mixed gases are ejected into the nozzle and combustion occurs, creating an annular configuration that surrounds, melts, and accelerates the axially injected powder particles. Axial powder injection provides uniform placement of the powder into the center of the flame, avoiding complications typically associated with perpendicular powder injection. The maximum flame temperature can approach 4500 ft/sec, whereas conventional combustion flame velocity is in the range of 300 to 500 ft/sec. The gun parameters that can be varied are oxygen flow, fuel gas flow, air flow, and gun hardware, and the deposition process variables are spray distance and spray rate. Propylene fuel gas was used for this study.

The plasma system used in this program was the Metco 9MB system. The plasma gun consists of an annular, water-cooled copper anode and a cone-shaped tungsten cathode, which is also water cooled. The plasma gases, usually inert, are passed between the cathode and anode where the plasma is initiated by an arc discharge, after which the stabilized plasma is maintained by a low-voltage, high-current discharge. The arc power influences the coating quality and deposition efficiency by affecting the heat available for melting of the powder. The arc power should be sufficient to melt the powder particles, but not too excessive to cause vaporization. The heat available in the plasma to melt the powder is also determined by the plasma gases, with a maximum plasma temperature being approximately 15,000 °C. Typically, a combination of gases, such as argon for the primary gas and hydrogen or helium for the secondary gas, is used for most plasma spraying processes.

A high-energy plasma, which has been optimized for the deposition of carbide systems, was used for this study. The high-energy plasma condition utilizes helium (monatomic) as the secondary gas, thereby maintaining a somewhat cooler plasma than hydrogen (diatomic), *i.e.*, 10,000 °C, and a high argon primary flow with a small bore nozzle to provide higher plasma flame velocities.

Powder and coating samples were analyzed for elemental chemistry and crystallographic phase composition. Inductively coupled plasma (ICP) and combustion methods were used to determine the metallic elements and carbon content, respectively. Inductively coupled plasma was performed using a Perkin-Elmer Plasma 2000 emission spectrometer, and the combustion measurements were performed using a Leco CS-444 analyzer. X-ray diffraction was conducted using a Philips APD 3520 diffractometer at a scanning rate of 0.5 degrees/min and with copper radiation.

Differential thermal analysis (DTA) is a method of determining the temperature at which thermal reactions occur in a material undergoing continuous heating or cooling. The nature, *i.e.*, exothermic or endothermic, and intensity of such reactions can also be determined. Differential thermal analysis was conducted on the starting powder as well as the HEP and HVOF coatings. The analysis was conducted using a 10 °C/min heat up from 25 to 1100 °C in an argon atmosphere. Coating samples were first pulverized into a powder, and each test was conducted using 320 mg of material. The samples were analyzed using X-ray diffraction after completion of DTA to determine the phase changes.

After determining the transformation temperature from DTA, coating samples were exposed to a furnace heat treatment in an argon environment. The heat treatment temperatures were chosen to be below (600 °C), at (870 °C), and above (1100 °C) the transformation temperatures determined via DTA. The heat treatment times ranged from 5 min to 1 hr. The samples were then examined using metallography, X-ray diffraction, and abrasive wear testing.

Samples of as-sprayed HVOF coating was removed from the substrate, and transmission electron microscopy (TEM) samples were prepared using an ultrasonic disk cutter. The thickness of the disks were reduced from the substrate side by grinding to a thickness of 300 μm. The ground samples were dimpled on both

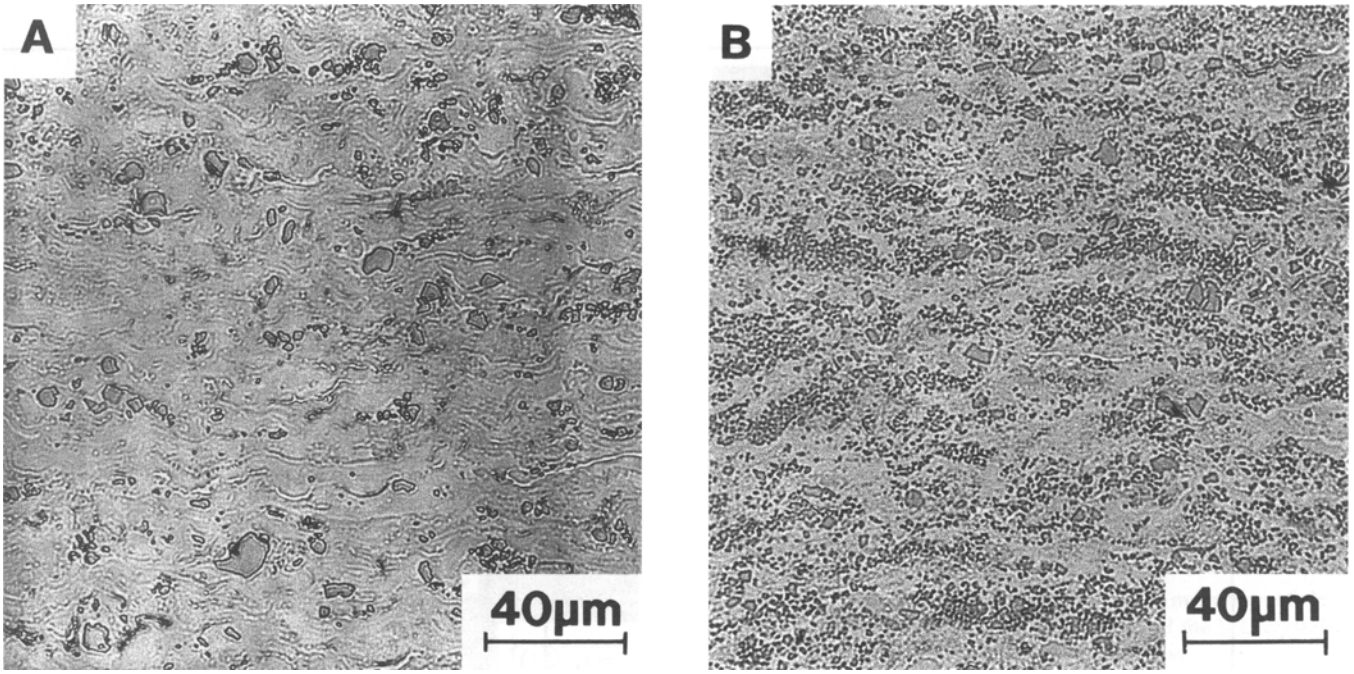

Figure 2 Optical photomicrographs of the coating cross sections that show the relative volume percentage of retained carbide phase (dark gray phase) for (a) HEP sprayed coating and (b) HVOF sprayed coating.

sides using a dimple grinder and subsequently thinned to perforation by ion milling. This procedure exposed the middle region of the coating to TEM analysis, thereby giving a representation of the bulk properties of the coating. The first few splat layers deposited during spraying are expected to experience a higher degree of rapid solidification than the subsequent layers of the bulk coating. It was felt, therefore, that examination of a coating region close to the substrate would not give adequate representation of the true state of the coating. The ion-milled specimens were then examined in a Hitachi H-800, 200 KeV scanning transmission electron microscope.

3. Results and Discussion

Optical photomicrographs of HEP and HVOF coatings in the as-sprayed condition are shown in Fig. 2(a) and (b), respectively. Samples were prepared by cold epoxy mounting of coating cross sections. The sample mounts were then course ground to a flat surface, rough sanded on a wheel with successively finer sand paper to 600 grit followed by polishing with 6-, 3-, and 1-μm diamond on a silk screen and finished with a relief polish with 0.3-μm alumina on a high nap cloth. The HVOF coating clearly contains a much higher concentration of tungsten monocarbide crystals (WC), as distinguished by the higher proportion of dark gray phase than the HEP coating. X-ray diffraction analysis (Fig. 3) confirmed the presence of a larger percentage of WC in the HVOF vs HEP coatings. This result was expected due to the higher flame velocity and lower flame temperature of the HVOF process, which would limit the decomposition process. X-ray diffraction also indicated a substantial amount of W_2C and elemental tungsten (W), but did not reveal substantial amounts of cobalt-containing subcarbides in the as-sprayed coatings, *i.e.*, Co_3W_3C, Co_6W_6C, Co_2W_4C, etc.

Chemical analysis (Table 2) indicated a substantial carbon loss (33 % for both HEP and HVOF coatings compared to the starting powder. The loss of carbon due to oxidation during spraying was expected and has been noted previously.[4] Based on the optical and X-ray diffraction analyses, it was expected that the HEP coating would contain less carbon due to its lower tungsten carbide content. It can be noted from Table 2 that both coatings possess the same carbon content; therefore, the HEP coating contains excess carbon in the coating, which is not in the form of a carbide. The results of chemical analysis also indicated the presence of cobalt in the coating (as expected), but X-ray diffraction did not reveal any substantial cobalt-containing phases. Instead, it showed a broad maxima in the 38 to 46 two theta range, which is characteristic of microcrystalline or amorphous material. The cobalt and excess carbon is present in the coatings in an amorphous state. It was also noted that there was less cobalt present in the HEP coating compared to the HVOF coating. This was attributed to the vaporization of cobalt in the hotter HEP flame.

Any cobalt that is in an amorphous state would recrystallize into cobalt-containing phases if heated to a sufficient temperature. Samples of feedstock powder, HEP and HVOF coatings underwent DTA to determine the temperature of the recrystallization reactions. Figure 4 shows the DTA charts indicating a large exothermic reaction at 853 °C for the HVOF and 860 °C for the HEP coatings, but only a slight endothermic reaction at 814 °C for the feedstock powder. This indicates that the exother-

Table 2 Results of Chemical Analysis

Sample	Composition, wt.% W	Co	O	C
Starting powder	82.90	11.61	.6187	4.09
HVOF coating	84.38	12.98	.1710	2.54
HEP coating	87.38	9.22	.1570	2.52

Table 3 Results of DTA

Sample	Reaction type	Reaction temperature,°C	Temperature differential,°C/mg (min)
Starting powder	Endothermic	814	Negligible
HVOF coating	Exothermic	853	0.02172
HEP coating	Exothermic	860	0.01764

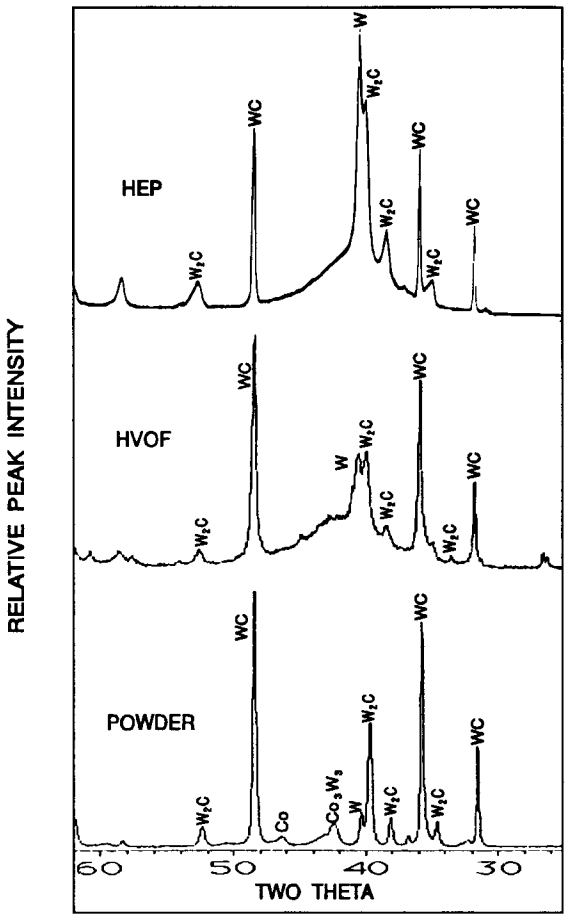

Figure 3 X-ray diffraction patterns for the HEP and HVOF as-sprayed coatings and feedstock powder. A broad maxima between 38 to 46° twoθ can be seen for both HEP and HVOF coatings.

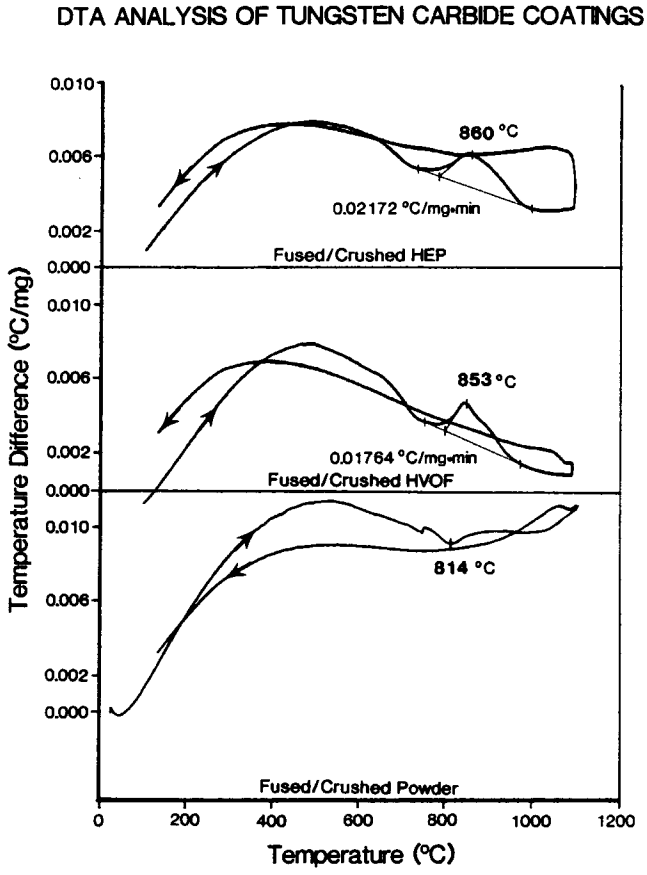

Figure 4 Differential thermal analysis of the feedstock powder, HVOF, and HEP coatings. Results indicate a strong exothermic reaction for the coatings at 853 and 860 °C, respectively.

mic reaction is inherent to the coatings, giving strong evidence that the reaction was the recrystallization of the amorphous material formed during spraying. The calculated magnitude, as determined by the temperature differential, for the HEP coating reaction was 25% greater than for the HVOF coating (Table 3), indicating that the as-sprayed HEP had more amorphous material. X-ray diffraction of coating samples after DTA showed the presence of a large amount of cobalt-containing phases (Co_6W_6C, Co_2W_4C) not present in the as-sprayed coatings and the elimination of the broad maxima.

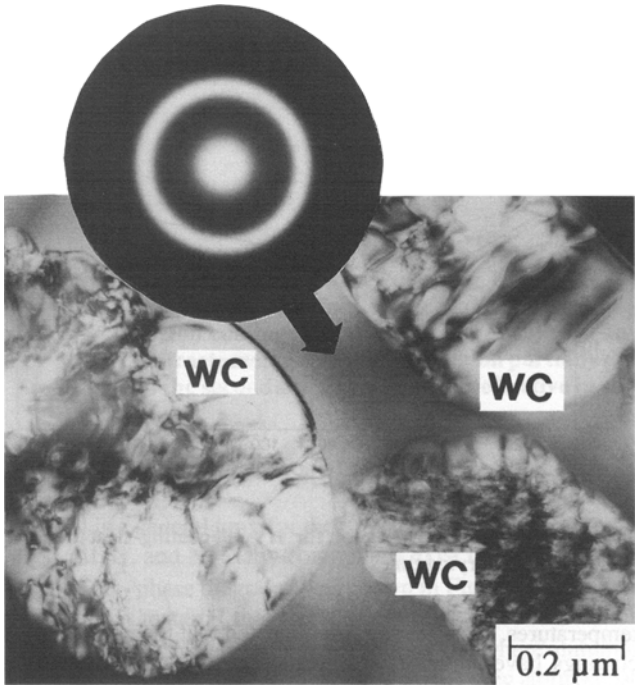

Figure 5 Bright field transmission electron micrograph showing crystalline WC particles embedded in an amorphous matrix. The microdiffraction pattern (inset) from the matrix consists of a series of concentric rings, which indicate amorphicity.

The microstructure of the as-sprayed HVOF sample as revealed by bright field TEM analysis is given in Fig. 5 and consists of crystalline particles embedded in a dark gray matrix. Microdiffraction determined that the crystalline particles were hexagonal WC with a *c/a* ratio of 0.97 and hexagonal W_2C with a *c/a* ratio of 1.57. There was a high density of dislocations and stacking faults for the crystalline WC particles, possibly created by stresses caused by impact during the spray process. The microdiffraction pattern (Fig. 5 inset) obtained from the matrix consists of a series of concentric diffuse rings characteristic of an amorphous phase. Other indications suggestive of an amorphous phase were the absence of diffraction contrast and lack of features in the bright field images. Qualitative analysis of several TEM samples of HVOF coating suggested that approximately 50 vol% of the coating consisted of amorphous material. It is noted, however, that the area of analysis for TEM samples is very small; therefore, an absolute percentage could not be determined.

Further analysis revealed areas of the matrix that contained very fine-grained crystals, usually concentrated about WC crystals (Fig. 6). These grains may be elemental tungsten formed from the decarburization of the WC crystals according to the oxidation mechanism proposed in the introduction. Elemental tungsten will nucleate and grow at the expense of the WC surface as carbon is depleted from the WC crystal surface. The round shape of grains at the WC surface agrees with classical nucleation and growth theory, *i.e.*, minimization of surface energy per unit volume. These grains have been "frozen" in mid-transformation due to rapid solidification and, therefore, cling to the WC crystal.

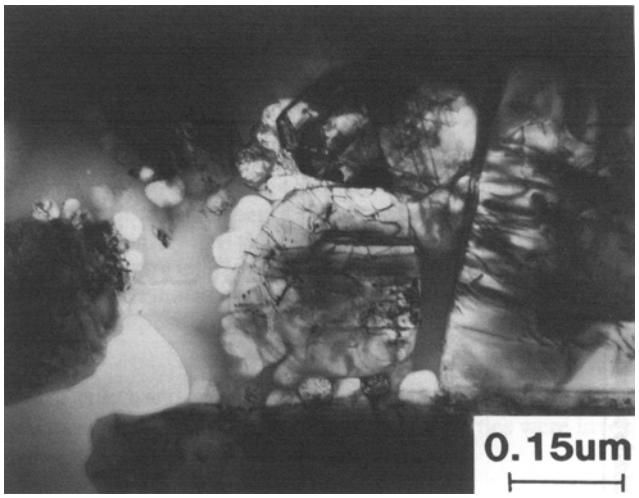

Figure 6 Bright field TEM image showing the nucleation of elemental tungsten which grows at the expense of the WC crystals due to oxidation during the thermal spray process.

Figure 7 is the X-ray diffraction pattern for the complete series of heat treatment temperatures for the HEP coating. The results for the HVOF coatings showed similar results. Samples heat treated at 600 °C, below the recrystallization temperature, showed no evident phase change from the as-sprayed coating (Fig. 3). Heat treatment at a temperature above recrystallization resulted in the transformation of the amorphous material into Co_6W_6C and Co_2W_4C with the Co_2W_4C phase becoming more predominate at the higher temperature. The tungsten monocarbide (WC) and elemental tungsten (W) content did not appear to change after the heat treatments, but the W_2C phase could not be detected at 1100 °C.

Previous work has based the wear performance on the volume percentage of carbide phase. Thus, it was expected that recrystallized coatings would have a higher wear resistance due to the additional carbide phases. Abrasive wear testing was performed on HVOF samples that were exposed to heat treatments for various times at a temperature above recrystallization, *i.e.*, at 900 °C. The results are presented in Fig. 8 and show an immediate improvement in wear resistance after a 5-min heat treatment. The improvment results from the rapid formation of new carbide phases during recrystallization. Depending on the time and temperature, different amounts and types of carbides can be formed during the recrystallization process resulting in the different improvements in wear resistance, as shown in Fig. 8.

4. Conclusion

It has long been noted that X-ray diffraction results on thermally sprayed tungsten carbide coatings contained a broad maxima in the 38 to 46 two θ region. The combined results of DTA, TEM, heat treatment, and X-ray diffraction indicate that the broad maxima is, in fact, amorphous material created by the diffusion of carbon and tungsten into the cobalt matrix and subsequent rapid solidification inherent to the thermal spray proc-

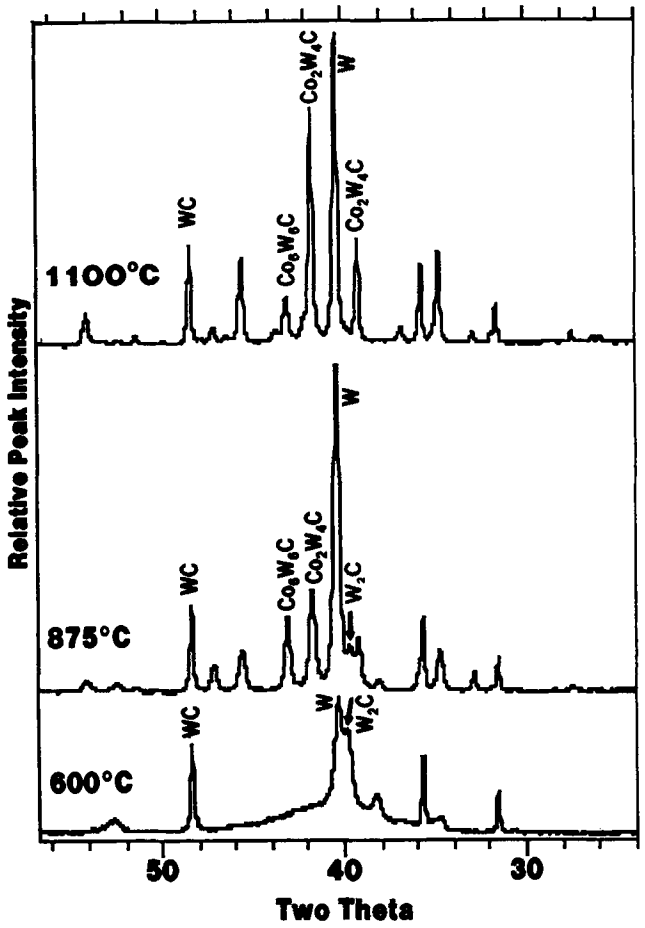

Figure 7 X-ray diffraction patterns for HEP coatings heat treated at 600, 875, and 1100 °C in an argon atmosphere. The results indicate recrystallization of the amorphous matrix into Co_6W_6C and Co_2W_4C.

ess. The amorphous material was shown to recrystallize at approximately 860 °C into eta phase carbides (Co_6W_6C and Co_2W_4C), with the Co_2W_4C phase being more stable at higher

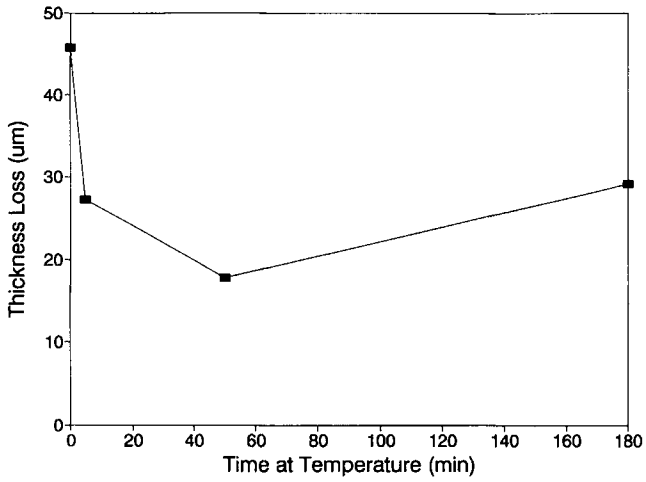

Figure 8 Thickness loss plot for HVOF coating heat treated at 900 °C for varying times.

temperatures. Wear testing has indicated that the recrystallized coatings have superior wear resistance compared to the as-sprayed coatings. The improvement in wear resistance is related to the precipitation of the eta phase carbides.

References

1. T.P. Slavin and J. Nerz, Material Characteristics and Performance of WC-Co Wear-Resistant Coatings, in *Thermal Spray Research and Applications*, T.F. Bernecki, Ed., ASM International, Materials Park (1991).
2. J. Nerz, B.A. Kushner, and A.J. Rotolico, Characterization of Tungsten Carbide Coatings As a Function of Powder Manufacturing and Deposition Technologies, in *High Performance Ceramic Films and Coatings*, Elsevier Science Publishers (1991).
3. V. Ramnath and N. Jayaraman, Characterization and Wear Performance of Plasma Sprayed WC-Co Coatings, *Mater. Sci. Technol.*, *5*, 382 (1987).
4. T.S. Chang and C. Kim, Tungsten Carbide Phase Transformation During Plasma Spray Process, *Am. Vac. Soc.*, P2479 (1985).